Available online at www.sciencedirect.com
SCIENCE DIRECT®
Scripta Materialia 52 (2005) 353–358
Scripta MATERIALIA
www.actamat-journals.com

Influence of tip bluntness on the size-dependent nanoindentation hardness ☆

Ju-Young Kim [a,b,*], Baik-Woo Lee [a], David T. Read [b], Dongil Kwon [a]

[a] School of Materials Science and Engineering, Seoul National University, San 56-1, Shillim-dong, Gwanak-gu, Seoul 151-744, South Korea
[b] Materials Reliability Division, National Institute of Standards and Technology, Boulder, CO 80305, USA

Received 10 August 2004; received in revised form 14 October 2004; accepted 29 October 2004
Available online 19 November 2004

Abstract

Nanoindenter tip bluntness modifies the size-dependent hardness relationship given by the Nix–Gao model. At shallow depths, fewer geometrically necessary dislocations are needed to accommodate the blunted tip. The experimentally measured ratio of plastic to total contact depth decreases and the hardness decreases relative to the idealized Nix–Gao model.

Keywords: Dislocation theory; Hardness; Nanoindentation; Tip bluntness

1. Introduction

Nanoindentation is used extensively to measure the hardness of materials. The hardness of a ductile metal is usually related to its compressive yield strength. However, the hardness values are commonly observed to depend on the indentation depth, especially in the nanometer range, so that they do not directly characterize material flow properties independent of indentation depth. To establish a useful correlation of hardness with material flow properties, it is essential to characterize the variation in hardness with indentation depth. An increase in hardness with decreasing indentation depth, the well-known indentation size effect (ISE), has been observed in numerous nanoindentation experiments on various materials [1–3]. This increase is believed to be associated with the geometrically necessary dislocations (GNDs) induced by imposed strain gradients [4–9]. Nix and Gao clearly showed the ISE for crystalline materials by considering the density of GNDs around a conical indenter [8]. The Nix–Gao model uses an ideally sharp indenter tip geometry, while some degree of bluntness is inevitable at the tip of a sharp indenter such as the Berkovich indenter generally used in nanoindentation experiments. Therefore, the Nix–Gao model does not completely describe the variation in hardness with indentation depth for depths less than about 100 nm [8–11]. This issue is critical in the ISE characterization of micromaterials, where the indentation depth is limited.

In this paper we present an improved ISE model that considers the effect of tip bluntness on the distribution of GNDs needed to accommodate a conical indenter with a blunt tip and the change in the ratio of plastic to total contact depth with contact depth. ISE depends on indenter tip shape since GNDs, the main cause of ISE, are required to accommodate the inhomogeneous plastic deformation at the surface caused by indentation. The actual indenter geometry is not self-similar, because of tip bluntness, so the ratio of plastic to total

☆ Partial contribution of the US National Institute of Standards and Technology. Not subject to copyright in the US.

* Corresponding author. Address: School of Materials Science and Engineering, Seoul National University, San 56-1, Shillim-dong, Gwanak-gu, Seoul 151-744, South Korea. Tel.: +82 2 880 8404; fax: +82 2 886 4847.
E-mail address: juyoung1@plaza.snu.ac.kr (J.-Y. Kim).

1359-6462/$ - see front matter
doi:10.1016/j.scriptamat.2004.10.036

contact depth at shallow contact depth changes with contact depth. We relate these two tip bluntness effects to parameters that are easily observed in the nanoindentation test, allowing convenient application of the present model. We show that the present model is in excellent agreement with nanoindentation results including contact depths less than 100 nm. We also show that the present model leads to a reasonable characteristic relation for the ISE.

2. Model

Fig. 1 shows schematically the nanoindentation contact morphology including pile-up for a conical indenter with a blunt tip, and the distribution of GNDs. We assume that the elastic recovery during unloading occurs only along the h direction (no change in contact radius, a) and uniformly with the ratio of plastic to total contact depth, χ, defined as

$$\chi = \frac{h_{c,off}}{h_c}, \tag{1}$$

where $h_{c,off}$ and h_c are the contact depths after unloading and at maximum load, respectively. χ is a ratio of lengths describing elastic recovery within the indentation zone. All lengths within the indentation zone and normal to the indentation direction are assumed to change by this ratio when unloading occurs. We assume that the indent after unloading is accommodated by circular loops of GNDs with Burgers vectors of magnitude b normal to the plane of the surface. GNDs are required to account for the inhomogeneous plastic deformation at the surface caused by indentation. We consider a blunted conical indenter with a primary angle, θ. The effective primary angle at maximum load, θ', falls below θ as the penetration depth decreases. The deformation described by the effective primary angle after unloading, θ'', is considered to result from GNDs. We think of the individual dislocation loops as being spaced equally along the angle θ'' in the region of $0 \leqslant r \leqslant a$, as shown in Fig. 1. From the definition of χ and geometric relations, we have

$$\tan\theta'' = \chi\tan\theta' = \frac{h_{c,off}}{h_c}\frac{h_c}{a} = \frac{b}{s}, \tag{2}$$

where s is the spacing between individual slip steps. If λ is the total length of the injected loops, the increment of λ between r and $r + dr$, $d\lambda$, is $2\pi r(dr/s)$, which gives the total length of GNDs after integration as

$$\lambda = \int_0^a 2\pi r\frac{1}{s}\,dr = \int_0^a 2\pi r\frac{\chi\tan\theta'}{b}\,dr = \frac{\pi a^2\chi\tan\theta'}{b} = \frac{\pi a\chi h_c}{b}. \tag{3}$$

Supposing that all of the injected loops remain within the hemispherical volume, $V = 2\pi a^3/3$, so the density of GNDs becomes

$$\rho_G = \frac{\lambda}{V} = \frac{3\chi h_c}{2ba^2} = \frac{3\chi}{2bh_c}\tan^2\theta'. \tag{4}$$

The density of GNDs in Nix–Gao model is $3\tan^2\theta/2bh$. χ is less than 1 when elastic recovery occurs, θ' is smaller than θ by a geometric effect of the tip bluntness. Consequently, the present model underestimates the density of GNDs relative to the Nix–Gao model.

We use the Taylor relation for shear strength τ to estimate the deformation resistance. We assume that the von Mises flow rule applies and that Tabor's factor of 3 can be used to convert the equivalent flow stress σ to hardness [8]. Thus hardness H is expressed as

$$H = 3\sigma = 3\sqrt{3}\tau = 3\sqrt{3}\alpha\mu b\sqrt{\rho_S + \rho_G}, \tag{5}$$

where ρ_S is the density of statistically stored dislocations, μ is the shear modulus, and α is the geometric constant. We consider ρ_S as independent of the indentation depth and α is 0.5 [8]. Using Eqs. (4) and (5), we can write the hardness as

$$\frac{H}{H_0} = \sqrt{1 + J\frac{h'}{h_c}}, \tag{6}$$

where H_0 is the macroscopic hardness in the absence of any GNDs ($H_0 = 3\sqrt{3}\alpha\mu b\sqrt{\rho_S}$) and h' is the characteristic length for the ISE, written as

$$h' = \frac{81}{2}b\alpha^2\tan^2\theta\left(\frac{\mu}{H_0}\right)^2. \tag{7}$$

H_0 and h' are constants of the material and primary indenter geometry, as in the Nix–Gao model, and a scaling factor J for the ISE has been introduced. From Eqs. (6) and (7), we have

$$J = \chi\left(\frac{\tan\theta'}{\tan\theta}\right)^2 = \chi\left(\frac{h_c}{h_c + \Delta h_b}\right)^2 = \chi\left(1 + \frac{\Delta h_b}{h_c}\right)^{-2}, \tag{8}$$

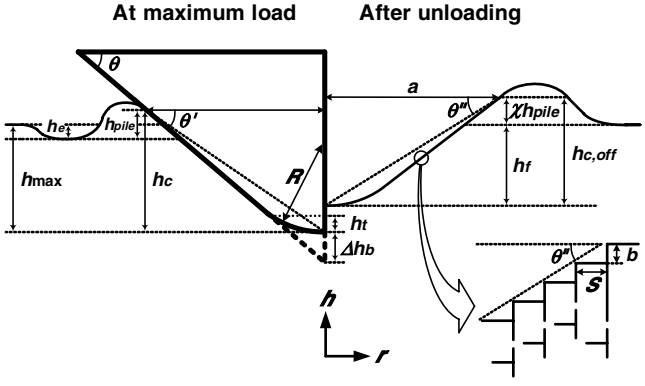

Fig. 1. Nanoindentation contact morphology including pile-up for a conical indenter with a blunt tip, and the distribution of geometrically necessary dislocations.

where Δh_b is the height difference between the sharp tip and the blunt tip. The χ term involves the elastic recovery effect by the tip bluntness, while the $(1 + (\Delta h_b/h_c))^{-2}$ term involves a geometric effect of the tip bluntness. χ is a function of contact depth, since the indenter geometry is not self-similar at shallow contact depth because of the tip bluntness effect. The $(1 + (\Delta h_b/h_c))^{-2}$ term reflects the correction of Δh_b for the distribution depth of GNDs. The tip bluntness constant Δh_b, and H and χ values measured as functions of contact depth are needed to apply the present model. The Nix–Gao model corresponds to $J = 1$ for full range of contact depth. For an ideally sharp indenter, if elastic contact depth is excluded for the distribution depth of GNDs, J is a constant corresponding to the χ value for the elastic–plastic material property and the specific self-similar geometry of the primary indenter.

3. Experimental methods

For nanoindentation experiments we used a commercial nanoindentation instrument [12] with a depth resolution of 0.1 nm and a load resolution of 0.1 μN. Nanoindentation experiments using two diamond Berkovich indenters, A and B, were conducted on a fused quartz standard specimen at various contact depths (3–400 nm). We related the contact area A and the contact depth analyzed by the Oliver–Pharr method [13] to the equation

$$A = \pi \tan^2(90^\circ - \theta)(h_c + \Delta h_b)^2. \quad (9)$$

Fig. 2 shows the area function results from which we obtained the Δh_b values for the A and B indenters as 19 and 35 nm, respectively, with $\theta = 19.7^\circ$ for the Berkovich indenter. Two samples, annealed and strain-hardened Cu, were prepared from 99.99% pure polycrystalline

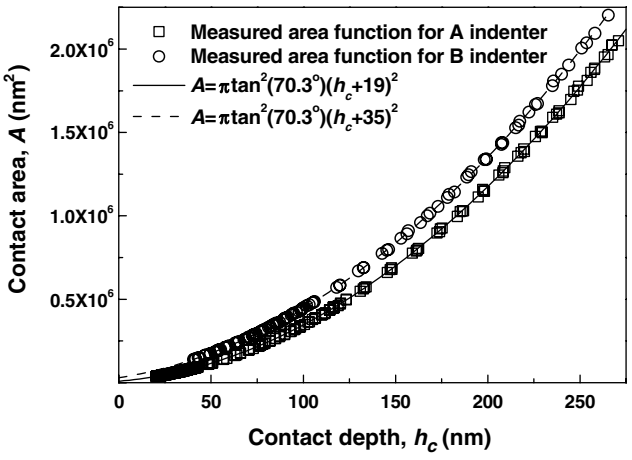

Fig. 2. Area functions of A and B indenters for determination the height difference between the sharp tip and the blunt tip, Δh_b.

Table 1
Properties of the samples

Material	Roughness (in $2000 \times 2000\,nm^2$) (nm)	E (GPa)	ν	μ (GPa)
Annealed Cu	7.78 ± 1.31	114.0	0.36	41.8
Strain-hardened Cu	8.35 ± 1.21	128.8	0.33	48.4

Cu. The sample surfaces were mechanically polished and then electropolished to remove the deformed layer. The grain size was sufficiently large compared to the indent produced by the high-load (~20 000 μN) nanoindentation experiments. The average surface roughness was measured by atomic force microscopy. The Young's modulus, Poisson's ratio, and shear modulus were measured by an ultrasonic pulse-echo technique, using a two-channel digital real-time oscilloscope. The measured properties of the samples are shown in Table 1.

Nanoindentation measurements were performed on both copper specimens using both indenters. Contact area was determined by the equation $A = \pi S^2/4E_{eff}$, where S is the contact stiffness measured during unloading, and E_{eff} is the effective elastic modulus [13]. E_{eff} was calculated using the measured Young's modulus and Poisson's ratio for the samples and a Young's modulus of 1140 GPa and a Poisson's ratio of 0.07 for the diamond indenter [13]. Hardness was determined from $H = P_{max}/A$, where P_{max} is the maximum load. Contact depth h_c was determined by inputting the calculated A to the area function, Eq. (9). Elastic deflection depth h_e was estimated by $h_e = 0.75(P_{max}/S)$ [14]. By the assumption of uniform elastic recovery discussed above, the ratio of lengths in the loaded state, $h_c/(h_{max} - h_e)$, is expected to be the same as the ratio of lengths in the unloaded state, $h_{c,off}/h_f$, where h_{max} and h_f are the maximum and final indentation depths as reported by the nanoindentation equipment. Equating these two ratios and using the definition of χ leads directly to the relation,

$$\chi = \frac{h_{c,off}}{h_c} = \frac{h_f}{h_{max} - h_e}, \quad (10)$$

which applies regardless of pile-up.

4. Results and discussion

The χ value for an ideally sharp indenter is a constant since the indenter geometry is self-similar for the full range of contact depth [2]. Fig. 3 shows that the measured χ value decreases as contact depth decreases at shallow contact depths. We believe that this decrease is a consequence of tip bluntness: specifically, the indenter geometry is not self-similar at shallow contact depths. The reference χ value for the self-similar Berkovich indenter geometry, χ_0, is measured at contact depth sufficiently large compared to the blunt tip–conical

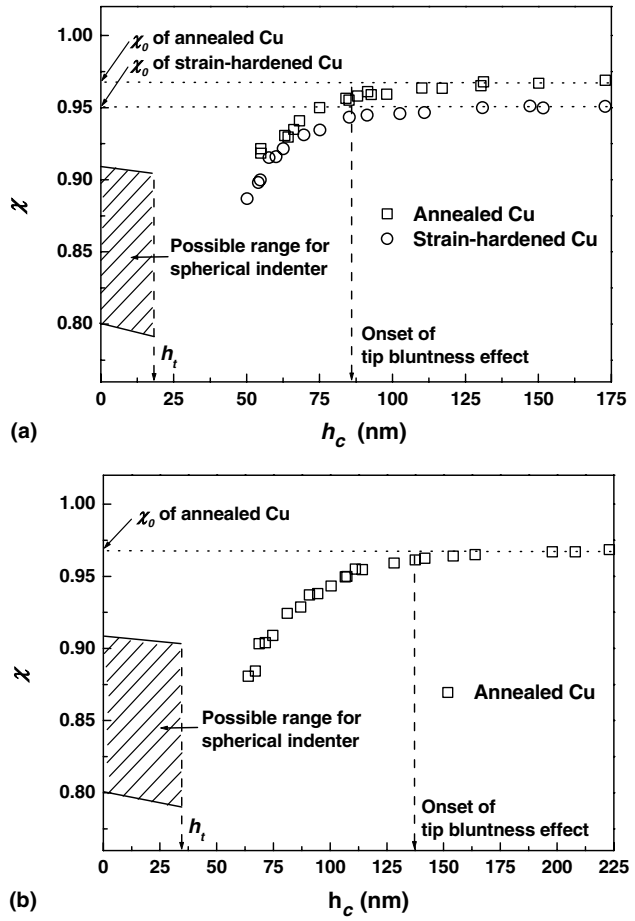

Fig. 3. χ results with contact depth and possible range of χ value calculated for the spherical tips of: (a) A and (b) B indenters.

indenter transition contact depth, h_t, as shown in Fig. 1. Our measured χ_0 values for annealed and strain-hardened Cu are 0.967 and 0.95, respectively. The criterion for the onset of tip bluntness effect is taken as $\chi/\chi_0 = 0.99$; the corresponding contact depths for the A and B indenters are 86 nm and 137 nm, respectively.

By considering the behavior of a spherical indentation for the blunt tip region, we can estimate a possible range of χ in the region of $0 < h_c \leqslant h_t$. The deformation state of the material directly beneath the spherical indenter changes from the fully elastic regime to the fully plastic regime as the penetration depth increases [17]. The criterion for the onset of fully plastic deformation under a spherical indenter is experimentally observed to be $a/R = 0.03$, where R is the indenter radius [9]. Considering that the radius of a blunted Berkovich indenter tip is from a few tens to a few hundreds nanometer [11,18], the contact depth corresponding to the fully elastic or the elastic–plastic transition regime is less than 1 nm. Therefore, we can conclude that the fully elastic and the elastic–plastic transition regimes are not relevant in nanoindentation experiments using Berkovich indenter, and we need only consider the fully plastic behavior. Making an estimate of the possible range of χ in the spherical tip region is simplified by this conclusion, since the variation of χ in the fully plastic regime is much less than in the fully elastic regime or the elastic–plastic transition regime. Because of elastic recovery during unloading, the radius of curvature of the spherical indentation trace, R_p, is generally found experimentally to be 10–25% greater than the indenter radius [9]. From these experimental results and geometric relations in Fig. 4, two equations, $a^2 = 2h_cR - h_c^2$ and $a^2 = 2h_cR_p - h_{c,off}{}^2 = 2h_cpR - h_{c,off}{}^2$, where p is a proportional constant between 1.1 and 1.25, are obtained by assuming no change in contact radius. The quantity $h_{c,off}/h_c$, which is equal to χ by definition, is calculated from these relationships. This calculation provides the possible range of χ value in the region of $0 < h_c \leqslant h_t$, as shown in Fig. 3, and gives χ values at h_t for both indenters between 0.79 and 0.90.

These values are used to interpret the observed behavior of χ, plotted in Fig. 3, as follows: as the penetration depth decreases, the blunt indenter tip begins to act like a spherical indenter rather than a sharp pyramidal indenter. The χ value decreases gradually from a reference value for a self-similar pyramidal indenter, χ_0, toward a lower value characteristic of a spherical indenter. The materials that reveal clear ISE phenomenon are intrinsically soft crystalline materials [8] in which χ_0 is usually close to 1 [1,2,13,15]. For these materials, χ is expected to decrease as contact depth decreases because of the tip bluntness effect. We note that contact depth used for ISE characterization should be at least a few times greater than h_t because ISE characteristic values are for a self-similar primary indenter.

Fig. 5 shows the hardness results for annealed Cu obtained using the A and B indenters. These two sets of hardness values are clearly distinguishable at contact depth less than the onset depths of the tip bluntness effect. Curves calculated using the present model, and $J = 1$ (the Nix–Gao model) are shown in Fig. 5. The present model curves fit the hardness results for annealed Cu for both indenters over the full range of contact depth; the acquired H_0 and h' values are 0.846 GPa and 463 nm for the A indenter and 0.842 GPa and 472 nm for the B indenter, respectively. The H_0 and h'

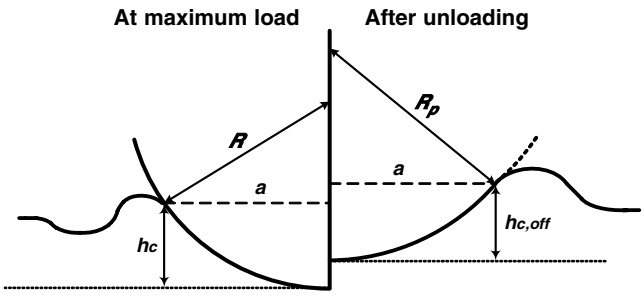

Fig. 4. Contact morphology of a spherical indenter.

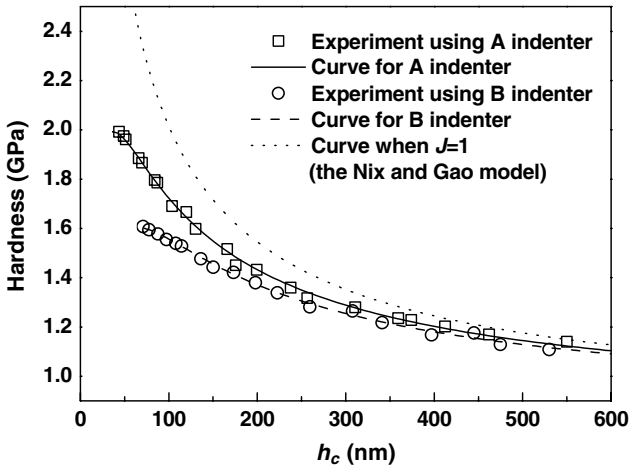

Fig. 5. Hardness results with contact depth and curves fitted by the present model for annealed Cu using A and B indenters.

values obtained using indenters with different tip bluntness are in good agreement despite the increasing differences in hardness values at shallow contact depths.

To test what might happen when indentation depth is limited to small values, we apply the present model to hardness results for contact depth less than the criteria listed above for the onset of tip bluntness effect. The results for H_0 and h' are 0.798 GPa and 538 nm for A indenter and 0.820 GPa and 505 nm for B indenter. These macroscopic hardness values and characteristic lengths for the ISE agree reasonably with those obtained using results from the full range of contact depth.

Fig. 6 shows two sets of nanoindentation results taken using indenter A, for annealed and strain-hardened Cu. The curves calculated using the present model reproduce the experimental hardness results over the full range of contact depth. To verify the measured h' values, we calculate h' using Eq. (7) as shown in Table 2. α is

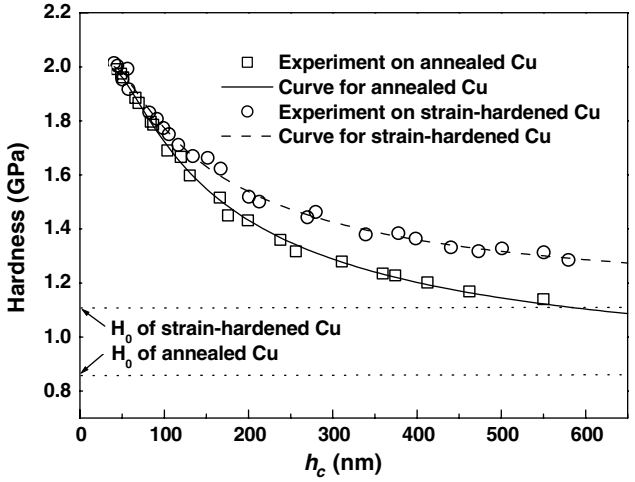

Fig. 6. Hardness results with contact depth and curves fitted by the present model for annealed and strain-hardened Cu.

Table 2
Measured and predicted characteristic values for indentation size effect

Material	Indenter	χ_0	H_0 (GPa)	h' (nm)	h' (predicted) (nm)
Annealed Cu	A	0.967	0.846	463	811
	B	0.967	0.842	472	819
Strain-hardened Cu	A	0.95	1.108	234	634

usually in the range of 0.3–0.6 for FCC metals [16]. Predicted values of h' from Eq. (7) are in reasonably good agreement with the measured values, considering that only a rough estimate of the value of the geometrical factor α is available.

5. Summary

We have improved the ISE model to include the effect of indenter tip bluntness based on GND theory. We applied the present model to hardness results for annealed Cu, obtained using two Berkovich indenters with different tip bluntness. We obtained similar H_0 and h' values despite the increasing differences in hardness results with decreasing contact depth. We also applied the present model to annealed and strain-hardened Cu. We observed good fits between the present model and the hardness results over the full range of contact depth; the fitting parameters provided consistent estimates of both the macroscopic hardness and the characteristic lengths for the ISE.

Acknowledgments

This research was supported by a grant (code #: 04K1501-01210) from the Center for Nanostructured Materials Technology under 21st Century Frontier R&D Programs of the Ministry of Science and Technology, Korea.

References

[1] Ma Q, Clarke DR. J Mater Res 1995;10:853.
[2] McElhaney KW, Vlassak JJ, Nix WD. J Mater Res 1998;13:1300.
[3] Krell A, Schadlich S. Mater Sci Eng 2001;A307:172.
[4] Fleck NA, Hutchinson JW. J Mech Phys Sol 2001;49:2245.
[5] Gao H, Huang Y, Nix WD, Hutchinson JW. J Mech Phys Sol 1999;47:1239.
[6] Huang Y, Gao H, Nix WD, Hutchinson JW. J Mech Phys Sol 2000;48:99.
[7] Elmustafa AA, Stone DS. J Mech Phys Sol 2003;51:357.
[8] Nix WD, Gao H. J Mech Phys Sol 1998;46:411.
[9] Swadener JG, George EP, Pharr GM. J Mech Phys Sol 2002;50:681.
[10] Zhang T-Y, Xu W-H, Zhao M-H. Acta Mater 2004;52:57.

[11] Wei Y, Wang X, Zhao M. J Mater Res 2004;19:208.
[12] Triboscope, Hysitron Inc.
[13] Oliver WC, Pharr GM. J Mater Res 1992;7:1564.
[14] Oliver WC, Pharr GM. J Mater Res 2004;19:3.
[15] Bolshakov A, Pharr GM. J Mater Res 1998;13:1049.
[16] Wiedersich H. J Met 1964;16:425.
[17] Tabor D. The Hardness of Metals. Oxford: Clarendon Press; 1951.
[18] Gouldstone A, Koh H-J, Zeng K-Y, Giannakopoulos AE, Suresh S. Acta Mater 2000;48:2277.